APPLIED PHYSICS

Exploiting extraordinary topological optical forces at bound states in the continuum

Haoye Qin[1], Yuzhi Shi[2]*, Zengping Su[1], Guodan Wei[1], Zhanshan Wang[2], Xinbin Cheng[2], Ai Qun Liu[3], Patrice Genevet[4]*, Qinghua Song[1]*

Polarization singularities and topological vortices in photonic crystal slabs centered at bound states in the continuum (BICs) can be attributed to zero amplitude of polarization vectors. We show that such topological features are also observed in optical forces within the vicinity of BIC, around which the force vectors wind in the momentum space. The topological force carries force topological charge and can be used for trapping and repelling nanoparticles. By tailoring asymmetry of the photonic crystal slab, topological force will contain spinning behavior and shifted force zeros, which can lead to three-dimensional asymmetric trapping. Several off-Γ BICs generate multiple force zeros with various force distribution patterns. Our findings introduce the concepts of topology to optical force around BICs and create opportunities to realize optical force vortices and enhanced reversible forces for manipulating nanoparticles and fluid flow.

INTRODUCTION

Bound states in the continuum (BICs) in photonic crystal slabs (PhCSs) are known to reveal topological features in the far-field patterns of radiating polarization states (*1*–*5*). The polarization vectors will wind around the singular point induced by zero outgoing power, which can be characterized by topological charge of the polarization vortex (*1*, *6*–*10*). PhCSs supporting BICs have been used to realize ultralow threshold lasing action, and, by taking advantage of their topological nature, optical vortex beams can be generated in momentum space without the need to align preciously to a real-space center (*11*–*15*). In view of polarization singularities, breaking the in-plane inversion symmetry of the PhCS will result in splitting of the vortex point at BIC to two circular points and linear polarizations that are able to achieve full coverage of the Poincare sphere (*16*, *17*). Dynamics and evolution of the polarization singularities including spawning circular polarizations and annihilation of topological charge have further been studied by modifying in-plane symmetry and σ_z symmetry of PhCSs (*17*–*19*).

Besides the control of polarization state, amplitude, and phase of waves, PhCSs and metasurfaces have also been great candidates for exploiting optical forces, such as optical trapping, manipulation, and meta-vehicles (*20*–*27*). By tailoring the scattering direction and structural chirality, optically pumped vehicles, light sails, and motors for transportation of nanoparticles and space exploration have been proposed recently (*20*, *21*, *26*, *28*). PhCS, particularly the presence of etched holes on the slab, are remarkably suitable for optical trapping (*29*, *30*). Exploiting quasi-BICs to enhance further the electromagnetic field localization markedly increases the optical force perceived by the particles (*31*, *32*).

[1]Tsinghua Shenzhen International Graduate School, Tsinghua University, Shenzhen 518055, China. [2]Institute of Precision Optical Engineering, School of Physics Science and Engineering, Tongji University, Shanghai 200092, China. [3]School of Electrical and Electronic Engineering, Nanyang Technological University, Singapore 639798, Singapore. [4]Université Côte d'Azur, CNRS, Centre de Recherche sur l'Hétéro-Epitaxie et ses Applications, Rue Bernard Gregory, Sophia Antipolis, Valbonne 06560, France.
*Corresponding author. Email: yuzhi_shi01@163.com (Y.S.); patrice.genevet@crhea.cnrs.fr (P.G.); song.qinghua@sz.tsinghua.edu.cn (Q.S.)

Here, we introduce the idea of zero optical force by exploiting the analogy between topological polarization singularities and topological zero power radiation, thus defining a force singular point at which the optical force goes to zero. To demonstrate the existence of such force singular point, we studied the behavior of optical forces in the vicinity of BICs, especially the topology of the optical force distribution in the momentum space, and found similar behavior as the one prescribed by the polarization vectors winding around the polarization singular point. We thus exploit the momentum space BIC nonradiative property to produce momentum-dependent vanishing optical forces. By looking in more details on the topological nature of optical force at BIC, we found diverse patterns, including converging and radiating topology for trapping and repelling nanoparticles. We show that the force vectors can also wind around force zero and, thus, can be quantized by similar topological charge of force, which implies the robustness of the topological force against change of the structure's and targeted objects' parameters. With the introduction of displacement and twist in the PhCS structure, topological force can reveal various distribution patterns, such as the spinning cyclone, shifted force zero to the off-Γ point, and asymmetric three-dimensional trapping. Last, the topology of the optical force is further manipulated to achieve several off-Γ BIC–induced force zeros.

RESULTS

Design principle of BIC protected topological optical force

Figure 1A schematically presents the PhCS chosen to support controllable BIC mode. It consists of a dual layer metastructure designed to break the *z*-inversion symmetry. The interface is achieved by etching half the way on top and bottom two arrays of rotated square nanoholes. The lattice period is kept constant at 574 nm and made of silicon. The side length of the square nanoholes is chosen at 330 nm, and the overall slab thickness is fixed at 600 nm. The two holes of the PhCS can be twisted with a rotation of α_{top} for the top layer and α_{bot} for the bottom layer. Depending on the rotation angles, α_{top} and α_{bot}, two scenarios with untwisted and twisted PhCS are studied. We called the untwisted PhCS regime the

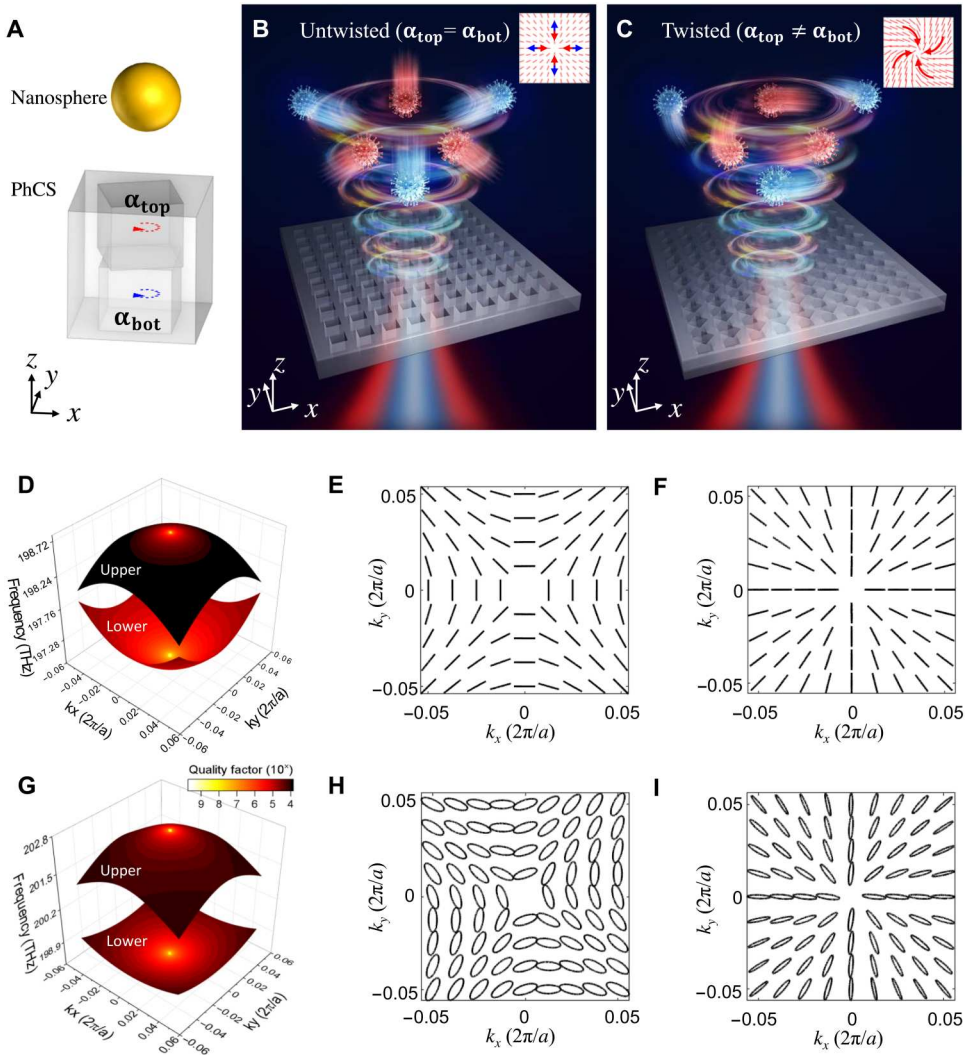

Fig. 1. BIC-induced topological distribution of optical force for manipulation of nanoparticles. (**A**) Schematic of a PhCS supporting BIC with topological optical force for trapping nanospheres in water. Holes in the PhCS can be twisted with a rotation angle of α_{top} for the top layer and α_{bot} for the bottom layer. (**B**) Illustration of topological force for trapping and dispersing nanoparticles on two bands with BICs in untwisted PhCS. (**C**) Topological force for trapping nanoparticles with spinning pattern in twisted PhCS. Insets in (B) and (C) show the distributions of force vectors in momentum space. With the twisted PhCS, nanoparticles will be trapped to or repelled from the center in a spinning feature like a swirl, which is different from the untwisted case leading to a rectilinear motion. (**D**) Iso-frequency surface and color-mapped quality factor of the untwisted PhCS for two eigenmodes ($\alpha_{top} = \alpha_{bot} = 0°$). Corresponding distribution of far-field polarization states of (**E**) the upper band (top) and (**F**) the lower band (bottom) in (D). (**G**) Iso-frequency surface and color-mapped quality factor of the twisted PhCS with $\alpha_{top} = 25°$, $\alpha_{bot} = 0°$ for two eigenmodes. Elliptical polarization states induced by the twist PhCS for (**H**) the upper band (top) and (**I**) the lower band (bottom) in (G).

condition $\alpha_{top} = \alpha_{bot} = 0^{\circ}$, that is, when the structure remains z-inversion symmetric and the twisted PhCS all other asymmetric conditions. For the trapping numerical analysis, we consider a polymeric nanosphere with a radius of 100 nm and a refractive index of 1.6 disposed at 1 μm above the center of the PhCS. The whole structure along with the nanosphere is immersed in water. Because of its topological nature in momentum space, BIC induces a force singular point named force zero ($\mathbf{F} = 0$), around which force distribution will have similar topology as far-field polarization states, hence trapping (repelling) the nanosphere at (off) the Γ point in an untwisted PhCS (Fig. 1B). This can be easily understood as the radiation field goes to zero at BIC, therefore forming a point with force also approaching zero (a force singular point). Whereas for a twisted PhCS, nanoparticles can be trapped in a spinning behavior (Fig. 1C). Figure 1D plots the calculated iso-frequency surfaces of two bands with their quality factors color-mapped for the untwisted PhCS. BIC with infinite quality factor is obtained at Γ point on each band. Note that the lower-band BIC quality factor decreases more slowly, improving the robustness against perturbation in the value of the momentum. The corresponding far-field polarization states are illustrated in Fig. 1 (E and F) with topological distribution, respectively, indicating that the upper- and lower-band BICs have opposite topological charge. In contrast, twisted PhCS can maintain BICs on the two bands as shown in Fig. 1G while generating elliptical polarization states with nearly the same ellipticity (Fig. 1, H and I). It is noteworthy that the solved eigenmodes of PhCS are unaffected by the introduced nanoparticles because the eigenfrequencies corresponding to

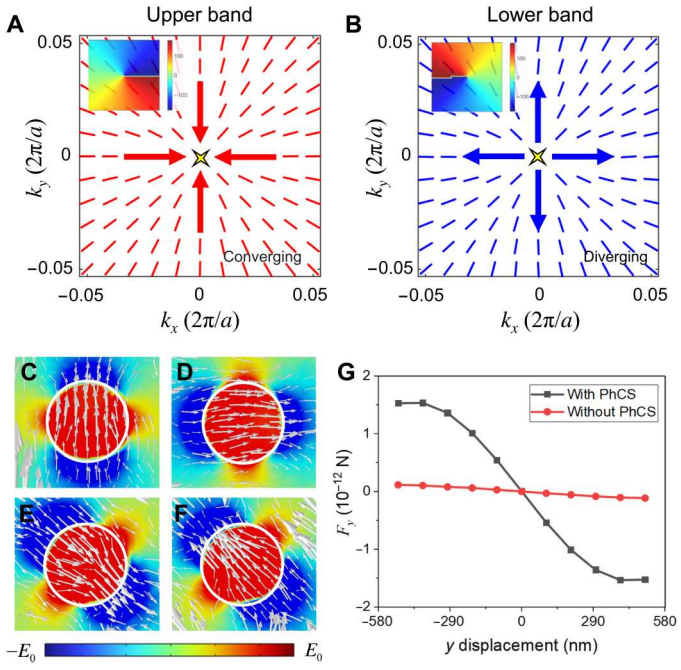

Fig. 2. Topological force distribution around BIC in momentum space with untwisted PhCS. BIC induces a force singular point (force zero, $F = 0$) at Γ point with topological distribution of optical force calculated by integrating MST surrounding a sphere 1000 nm above the PhCS for the (**A**) upper band and (**B**) lower band. (A) The upper band has optical forces converging toward the center, Γ point. (B) The lower band has optical forces radiating away from the center. Insets plot maps of the angle of the force vector $\phi_F(\mathbf{k})$ showing topological winding feature of optical force around BIC in momentum space. The converging and radiating force patterns are of rotation symmetry with a degree of 180. Lower-band Poynting vector and electric field profile around the nanosphere with (**C**) $k_x = 0$, $k_y < 0$ (**D**) $k_x < 0$, $k_y = 0$, (**E**) $k_x < 0$, $k_y > 0$, and (**F**) $k_x > 0$, $k_y < 0$. Here, E_0 is equal to 1×10^6V/m. (**G**) Comparison between magnitude of the converging force with a 10×10 PhCS and without PhCS by shining a Gaussian beam with a frequency of 186 THz, a beam width of 287 nm, and a focal plane at $z = 850$ nm.

the eigenmodes of the PhCS and nanoparticle are very different due to the large contrast in the shape, size, and index of the PhCS and nanoparticles. In addition, there is no mutual coupling due to their large enough distance. Therefore, BIC in the PhCS suffers no impact from the introduction and movement of the nanoparticles, paving the base for manipulating nanoparticles in motion. As for practical excitation of the BIC eigenmodes, a Gaussian beam can be used as incident light thanks to its decomposition to different values of in-plane vector $\mathbf{k}_{\|}$ (*3*, *11*, *13*, *14*). The different k components of the excitation beam would interact with different $\mathbf{k}_{\|}$ resonances of the PhCS, spawning the BIC topology and hence topological force.

To illustrate the BIC-induced topological force in momentum space for manipulating nanoparticles, we are calculating the net optical force on the nanosphere above PhCS as a function of the metastructure geometry. Rigorous calculation of optical forces on arbitrary sized and shaped particles can be obtained by integrating the flow of Maxwell stress tensor (MST) through a closed surface S containing the nanoparticle as follows (*21*, *24*, *33*)

$$\mathbf{F} = \oint_S \left\langle \overleftrightarrow{\mathbf{T}} \right\rangle \cdot \hat{\mathbf{n}} dS \qquad (1)$$

where $\hat{\boldsymbol{n}}$ is the unit vector normal to the surrounding surface S, and $\langle \cdot \rangle$ is the time-average operator. The MST can be given in the form of electric field $\mathbf{E}$ and magnetic field $\mathbf{H}$,

$$\langle T_{ij} \rangle = \frac{1}{8\pi} \Re \left[D_i E_j^* + B_i H_j^* - \frac{1}{2} (\mathbf{D} \cdot \mathbf{E}^* + \mathbf{B} \cdot \mathbf{H}^*) \delta_{ij} \right] \qquad (2)$$

Here, δ_{ij} is the Kronecker delta, and $\mathbf{D} = \varepsilon\mathbf{E}$, $\mathbf{B} = \mu\mathbf{H}$, with ε and μ denoting the permittivity and permeability of the medium, respectively. BIC feature of the PhCS can be seen from the infinite quality factor at Γ point in Fig. 1 (D and G), leading to zero radiated far-field power at this point. This zero radiation is demonstrated in the topological winding electric polarization distribution around Γ point in Fig. 1 (E and F) and Fig. 1 (H and I). Through stress tensor for optical force and winding polarization of BIC singular point, the correlation between the BIC and force zero can be established. The force zero can be achieved either (i) by using BIC that generates near-zero fields or (ii) by designing symmetric distribution of forces that cancel each other with opposite sign. For case (i), BIC results in zero radiation, that is, when both $\mathbf{E}$ and $\mathbf{H}$ simultaneously vanish. This is the obvious case with zero stress tensor and zero force integration. For the more subtle case (ii), the force can be arranged to distribute with inversion symmetry around one point, at which forces in opposite direction offset each other and spawning a force zero. Away from the zero-force singular point, we find that the topological winding electric polarization distribution also leads to a winding optical force with diverse manipulating features. To understand the force topology of the two cases, we write the force vector as $\mathbf{F}(\mathbf{k}) = F_x(\mathbf{k})\hat{\mathbf{x}} + F_y(\mathbf{k})\hat{\mathbf{y}}$, where $\mathbf{k} = k_x\hat{\mathbf{x}} + k_y\hat{\mathbf{y}}$ is the two-dimensional wave vector, and $F_{x,\,y}$ is the optical force in the x and y directions, respectively. The force topology is then characterized and quantized with topological charge as (*1*, *11*, *34*)

$$q_F = \frac{1}{2\pi} \oint_L d\mathbf{k} \cdot \nabla_{\mathbf{k}} \phi_F(\mathbf{k}) \qquad (3)$$

which describes how many times the force vector winds around the force zero. Here, $\phi_F(\mathbf{k}) = \arg[F_x(\mathbf{k}) + iF_y(\mathbf{k})]$ is the angle of the force vector in the momentum space. Although the proposed topological force is investigated in momentum space, it actually connects to real space based on the relation between the spatial angle and in-plane vector $\mathbf{k}_{\|}$ (see the Supplementary Materials).

Converging and diverging topological optical force

Figure 2 demonstrates the topological distribution of optical force in momentum space induced by the BIC singular point with untwisted PhCS. Figure 2 (A and B) shows the converging and diverging patterns of the optical force generated by the lower-band and upper-band BICs, respectively. Force converging toward BIC point is represented by red color, and the pattern indicates that when nanoparticles are located within the vicinity of the BIC point, they will perceive a moving and trapping force toward the Γ-BIC. This force is of interest for collecting and accumulating nanoparticles. As for the diverging force pattern, any off-Γ position will have a force that would repel objects away from the center. Insets in Fig. 2 (A and B) show that the angle of the force vector is topologically distributed in momentum space and confirm that the two patterns have an angle difference of 180°. The direction of the converging optical force can be illustrated by calculating the Poynting vector around the object. At a point of $k_x = 0$, $k_y < 0$, the

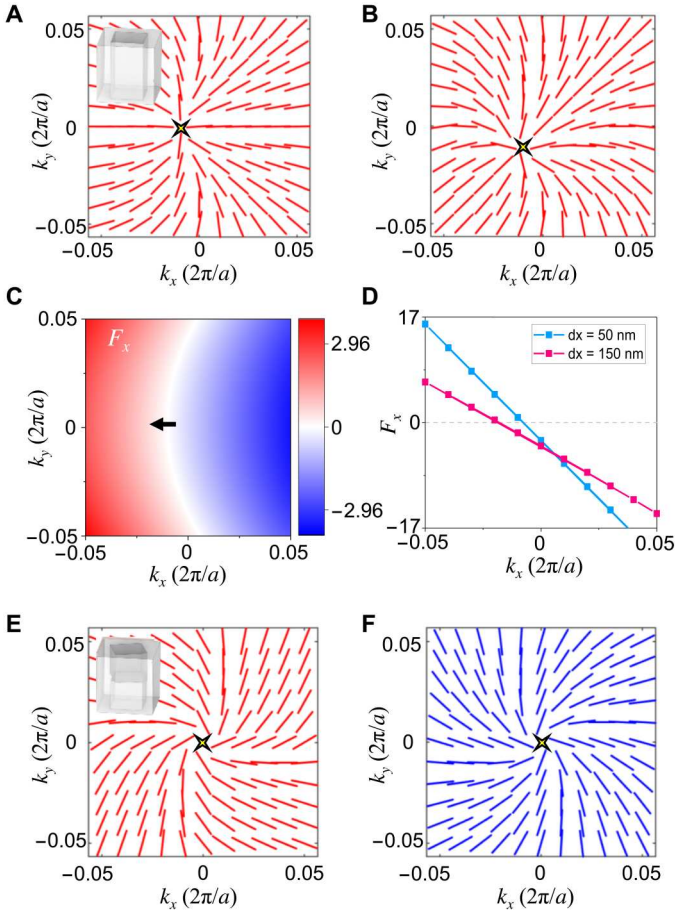

Fig. 3. Topological forces with perturbation. (**A**) Force distribution around lower-band BIC with untwisted PhCS when the nanosphere is displaced 100 nm along positive *x* axis. (**B**) Force distribution around lower-band BIC when the nanosphere is displaced both 100 nm along positive *x* axis and 100 nm along positive *y* axis. (**C**) Map of F_x in momentum space when the nanosphere is displaced 100 nm along positive *x* axis. The arrow indicates the shift of $F_x = 0$. (**D**) F_x as a function of k_x at $k_y = 0$ with the nanosphere displaced 50 and 100 nm along positive *x* axis. The optical forces in (C) and (D) are normalized to a value of $F_0 = 10^{-16}N$. Force distribution above the PhCS around (**E**) lower-band BIC and (**F**) upper-band BIC when the PhCS has a rotation angle with $\alpha_{top} = 25°$ and $\alpha_{bot} = 0°$. Insets in (E) show the structure of the perturbed PhCS.

Poynting vectors are pointing upward, meaning that the optical force is pushing the nanosphere toward $k_y = 0$, as shown in Fig. 2C. For $k_x < 0$, $k_y = 0$, the Poynting vectors are pointing toward right to bring the nanosphere toward $k_x = 0$, as shown in Fig. 2D. This behavior is confirmed by looking at the two-dimensional deviation in Fig. 2E ($k_x < 0$, $k_y > 0$) and Fig. 2F ($k_x > 0$, $k_y < 0$), where the nanoparticle always has Poynting vectors pointing to the BIC point. Figure 2G compares the optical force F_y perceived by a nanosphere alone and after placing a 10 × 10 PhCS excited by a Gaussian beam impinging at normal incidence. Without PhCS, the optical force is exclusively generated by the Gaussian beam. Whereas when there is a finite PhCS, the BIC topological optical force, mainly induced by the field enhancement of the BIC mode, is almost one order of magnitude higher than the one with only the Gaussian beam.

Topological optical force with symmetry breaking

To further demonstrate the effect of converging force, Fig. 3A plots the distribution of optical force and force zero with untwisted PhCS when the nanosphere is laterally displaced by about 100 nm in the positive *x*-axis direction. The force zero has a displacement toward negative k_x, and the topology reveals that the optical force converges toward the shifted off-Γ force zero. When the nanosphere is moving toward Γ point, force zero will approach Γ point on the other side, and the position of nanosphere and force zero will finally coalesce at Γ point, achieving optical trapping condition. Similar phenomenon occurs with force zero shifting along the negative direction of diagonal when displacing nanosphere 141 nm along the positive direction of diagonal (Fig. 3B). Figure 3C shows the force in the *x* direction for the case in Fig. 3A, where the force zero region bends toward the direction of negative k_x, as indicated by the arrow. Line plot of the force in *x* direction is shown in Fig. 3D with different displacement of $d_x = 50$ nm and $d_x = 150$ nm. Both lines cross zero at positions of $k_x \neq 0$, and for larger displacement, the line becomes more tilted toward negative direction. Engineering the PhCS to reveal diverse polarization features originating from the BIC topology and intriguing optical force distribution in momentum space around BIC are expected. To further demonstrate the design versatility offered by this approach, we conceived a PhCS unit cell containing rotated top hole disposed at an angle of 25° with respect to the hole orientation in the lower layer, thus forming a twisted PhCS. The calculated force patterns given in Fig. 3E for the upper band and in Fig. 3F for the lower band also enable a BIC-induced force zero at Γ point. With the twisted PhCS, nanoparticles will be trapped to or repelled from the center with a spinning feature like a swirl, which is different from the untwisted case with the point-to-point force leading to a rectilinear motion. This spinning force feature associated with twisted PhCS at BIC may lead to diverse possibilities in nanoparticle sorting, manipulating, and optofluidics.

Manipulation with multiple BICs

Modifying the lattice constant of untwisted PhCS to 517 nm, we achieved interesting off-ΓBICs from which we evaluate their topological forces in Fig. 4. We observe that the quality factor presents now four infinite points resulting from four BICs emerging symmetrically at $k_x = 0$ and $k_y = 0$. The corresponding force distribution is shown in Fig. 4B. Five force zeros are found, and four of them are directly attributed to the BIC modes observed in Fig. 4A. One exception related to the zero force at Γ point is attributed to the inversion symmetry. The four off-Γ force zeros introduce repelling force outward offset in the opposite direction one with respect to the others to form an additional force zero at the Γ point. The force zero at Γ point can be understood as a converging center, and the BIC points as radiating centers. The distribution of absolute value of optical force is shown in Fig. 4C in log scale, clearly indicating the five force zeros in momentum space. Map of the force angle $\phi_F(\mathbf{k})$ demonstrates the topological feature with charge of 1 for force zeros at BICs (white arrow) and opposite charge of −1 for force zero induced by symmetry (black arrow) as shown in Fig. 4D. Applying sign function to force in *x* and *y* directions results in Fig. 4 (E and F) illustrating the force direction, respectively. BICs generate triangle regions that drag objects to BICs in one direction and pulling them away in the other direction. Another eigenmode has several BICs forming a band that encloses the Γ point (Fig. 4G). In Fig. 4H,

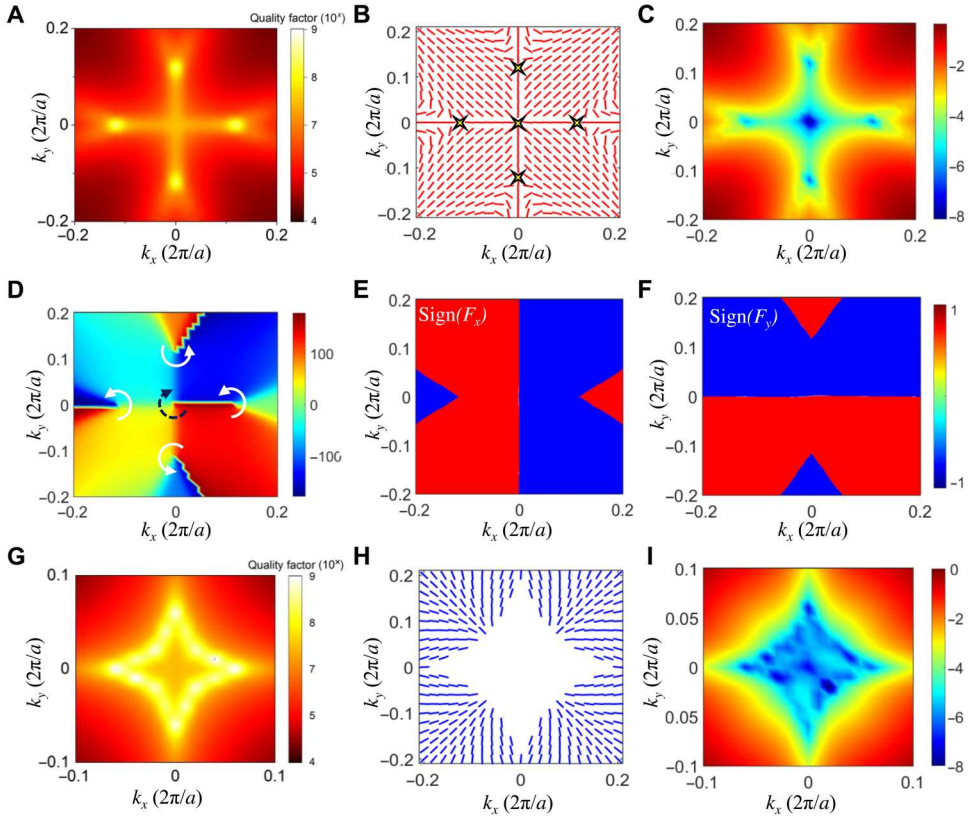

Fig. 4. Topological features of optical force around off-Γ BIC when the untwisted PhCS lattice constant is reduced to 517 nm. (**A**) Quality factor of one eigenmode showing that four off-Γ BICs are obtained. (**B**) Topological distribution of optical force surrounding four BICs. (**C**) Absolute value of optical force in log scale shows force zeros occurring at four BICs and one additional at Γ point. (**D**) Map of the value $\phi_F(\mathbf{k})$ showing topological features of optical force around force zeros in momentum space. The black and white arrows have opposite topological charge. Map of sign of (**E**) F_x and (**F**) F_y in momentum space. (**G**) Quality factor of another eigenmode shows several BICs enclosing the Γ point. (**H**) Distribution of optical force around these BICs. Accumulation of these singular points results in nearly zero force within a diamond-like region around the Γ point. (**I**) Map of absolute value of optical force in log scale around the accumulating BICs.

the force distribution is radiating outward and goes to zero within a diamond-like region around the Γ point. Absolute value of optical force of this band is given in Fig. 4I. Objects within the force zero region will be nearly stable, and objects outside can be pulling away, a behavior of great interest, for example, to sort and separate nanoparticles.

As for experimental realization, the PhCS can be made of silicon, silicon nitride, titanium dioxide, and other dielectric materials, which have been widely used to fabricate optical PhCSs and observe BIC effects. Here, we use silicon as the structure material and the geometrical parameters of the PhCS that are well compatible with nanofabrication approaches. The proposed PhCS of period larger than 500 nm can be fabricated with typical electron-beam lithography (EBL) and reactive ion etching process. We have also evaluated the trapping performance for different relevant particle types in terms of various refractive indices from 1.4 to 1.8 and various radii from 50 to 200 nm, and we find that the topological distribution of optical forces is stable and robust. We propose that the single layer PhCS can be fabricated by using conventional EBL and etching (*5*, *15*, *35*, *36*), followed by direct wafer bonding of two PhCS layers (*37*). Another option could consist in fabricating two layers via EBL, using planarization with spin on glass in between the two lithography steps (*38*, *39*).

DISCUSSION

In conclusion, we unveil the topological feature of optical force distribution in momentum space around BIC. We observe that the force vectors wind around the force singular point similarly as the phase that winds around optical singularities in photonics. We characterized these zero force singular points by a force topological charge and show that converging and diverging force patterns are associated with the same topological charge but with 180° angle difference. Being almost one order of magnitude higher than the Gaussian beam–induced optical forces, these force patterns distributed around force singularities have the capability of trapping and repelling nanoparticles. The topological force can also be engineered to manifest spinning vortices by modifying σ_z asymmetry of the PhCS. Off-Γ BICs generate multiple force zeros and enrich the force patterns for optical manipulation. This study may open up a new avenue for optical trapping and manipulation of nanoparticles using BIC topology and may also inspire the future development of nanosorters and nanorobots in microfluidic systems.

MATERIALS AND METHODS

The simulation results are performed by COMSOL Multiphysics software.

Supplementary Materials

This PDF file includes:

Notes S1 to S8
Figs. S1 to S13
References

REFERENCES AND NOTES

1. B. Zhen, C. W. Hsu, L. Lu, A. D. Stone, M. Soljačić, Topological nature of optical bound states in the continuum. *Phys. Rev. Lett.* **113**, 1–5 (2014).
2. L. Shi, Y. Kivshar, W. Liu, W. Liu, Topological polarization singularities in metaphotonics. *Nanophotonics* **10**, 1469–1486 (2021).
3. Y. Zhang, A. Chen, W. Liu, C. W. Hsu, B. Wang, F. Guan, X. Liu, L. Shi, L. Lu, J. Zi, Observation of polarization vortices in momentum space. *Phys. Rev. Lett.* **120**, 186103 (2018).
4. C. W. Hsu, B. Zhen, A. D. Stone, J. D. Joannopoulos, M. Soljacic, Bound states in the continuum. *Nat. Rev. Mater.* **1**, 16048 (2016).
5. J. Jin, X. Yin, L. Ni, M. Soljačić, B. Zhen, C. Peng, Topologically enabled ultrahigh-Q guided resonances robust to out-of-plane scattering. *Nature* **574**, 501–504 (2019).
6. H. M. Doeleman, F. Monticone, W. den Hollander, A. Alù, A. F. Koenderink, Experimental observation of a polarization vortex at an optical bound state in the continuum. *Nat. Photonics* **12**, 397–401 (2018).
7. T. Bai, Q. Li, Y. Wang, Y. Chen, Z.-D. Hu, J. Wang, Terahertz vortex beam generator based on bound states in the continuum. *Opt. Express* **29**, 25270–25279 (2021).
8. S. Joseph, S. Pandey, S. Sarkar, J. Joseph, Bound states in the continuum in resonant nanostructures: An overview of engineered materials for tailored applications. *Nanophotonics* **10**, 4175–4207 (2021).
9. S. Mohamed, J. Wang, H. Rekola, J. Heikkinen, B. Asamoah, L. Shi, T. K. Hakala, Controlling topology and polarization state of lasing photonic bound states in continuum. *Laser Photon. Rev.* **16**, 2100574 (2022).
10. Z. Chen, X. Yin, J. Jin, Z. Zheng, Z. Zhang, F. Wang, L. He, B. Zhen, C. Peng, Observation of miniaturized bound states in the continuum with ultra-high quality factors. *Sci. Bull.* **67**, 359–366 (2022).
11. B. Wang, W. Liu, M. Zhao, J. Wang, Y. Zhang, A. Chen, F. Guan, X. Liu, L. Shi, J. Zi, Generating optical vortex beams by momentum-space polarization vortices centred at bound states in the continuum. *Nat. Photonics* **14**, 623–628 (2020).
12. A. Kodigala, T. Lepetit, Q. Gu, B. Bahari, Y. Fainman, B. Kanté, Lasing action from photonic bound states in continuum. *Nature* **541**, 196–199 (2017).
13. L. Kang, Y. Wu, X. Ma, S. Lan, D. H. Werner, High-harmonic optical vortex generation from photonic bound states in the continuum. *Adv. Opt. Mater.* **10**, 2101497 (2022).
14. Y. Wu, L. Kang, D. H. Werner, Active quasi-BIC optical vortex generators for ultrafast switching. *New J. Phys.* **24**, 033002 (2022).
15. C. Huang, C. Zhang, S. Xiao, Y. Wang, Y. Fan, Y. Liu, N. Zhang, G. Qu, H. Ji, J. Han, L. Ge, Y. Kivshar, Q. Song, Ultrafast control of vortex microlasers. *Science* **367**, 1018–1021 (2020).
16. W. Liu, B. Wang, Y. Zhang, J. Wang, M. Zhao, F. Guan, X. Liu, L. Shi, J. Zi, Circularly polarized states spawning from bound states in the continuum. *Phys. Rev. Lett.* **123**, 116104 (2019).
17. T. Yoda, M. Notomi, Generation and annihilation of topologically protected bound states in the continuum and circularly polarized states by symmetry breaking. *Phys. Rev. Lett.* **125**, 053902 (2020).
18. Y. Zeng, G. Hu, K. Liu, Z. Tang, C. W. Qiu, Dynamics of topological polarization singularity in momentum space. *Phys. Rev. Lett.* **127**, 176101 (2021).
19. W. Ye, Y. Gao, J. Liu, Singular points of polarizations in the momentum space of photonic crystal slabs. *Phys. Rev. Lett.* **124**, 153904 (2020).
20. D. Andrén, D. G. Baranov, S. Jones, G. Volpe, R. Verre, M. Käll, Microscopic metavehicles powered and steered by embedded optical metasurfaces. *Nat. Nanotechnol.* **16**, 970–974 (2021).
21. O. Ilic, H. A. Atwater, Self-stabilizing photonic levitation and propulsion of nanostructured macroscopic objects. *Nat. Photonics* **13**, 289–295 (2019).
22. Y. Y. Tanaka, P. Albella, M. Rahmani, V. Giannini, S. A. Maier, T. Shimura, Plasmonic linear nanomotor using lateral optical forces. *Sci. Adv.* **6**, eabc3726 (2020).
23. M. Liu, T. Zentgraf, Y. Liu, G. Bartal, X. Zhang, Light-driven nanoscale plasmonic motors. *Nat. Nanotechnol.* **5**, 570–573 (2010).
24. Y. Shi, Q. Song, I. Toftul, T. Zhu, Y. Yu, W. Zhu, P. Tsai, Y. Kivshar, A. Q. Liu, Optical manipulation with metamaterial structures. *Appl. Phys. Rev.* **9**, 031303 (2022).
25. R. Quidant, A light ride to the stars. *Nat. Photonics* **13**, 227–228 (2019).
26. H. A. Atwater, A. R. Davoyan, O. Ilic, D. Jariwala, M. C. Sherrott, C. M. Went, W. S. Whitney, J. Wong, Materials challenges for the Starshot lightsail. *Nat. Mater.* **17**, 861–867 (2018).
27. O. Ilic, I. Kaminer, B. Zhen, O. D. Miller, H. Buljan, M. Soljačić, Topologically enabled optical nanomotors. *Sci. Adv.* **3**, 1–8 (2017).
28. X. Wu, R. Ehehalt, G. Razinskas, T. Feichtner, J. Qin, B. Hecht, Light-driven microdrones. *Nat. Nanotechnol.* **17**, 477–484 (2022).
29. T. van Leest, J. Caro, Cavity-enhanced optical trapping of bacteria using a silicon photonic crystal. *Lab Chip* **13**, 4358–4365 (2013).
30. A. S. Ang, S. V. Sukhov, A. Dogariu, A. S. Shalin, Scattering forces within a left-handed photonic crystal. *Sci. Rep.* **7**, 41014 (2017).
31. S. Yang, C. Hong, Y. Jiang, J. C. Ndukaife, Nanoparticle trapping in a quasi-BIC system. *ACS Photonics* **8**, 1961–1971 (2021).
32. Y. Shi, Y. Wu, L. K. Chin, Z. Li, J. Liu, M. K. Chen, S. Wang, Y. Zhang, P. Y. Liu, X. Zhou, H. Cai, W. Jin, Y. Yu, R. Yu, W. Huang, P. H. Yap, L. Xiao, W. Ser, T. T. B. Nguyen, Y. T. Lin, P. C. Wu, J. Liao, F. Wang, C. T. Chan, Y. Kivshar, D. P. Tsai, A. Q. Liu, Multifunctional virus manipulation with large-scale arrays of all-dielectric resonant nanocavities. *Laser Photon. Rev.* **16**, 2100197 (2022).
33. H. Li, Y. Cao, L.-M. Zhou, X. Xu, T. Zhu, Y. Shi, C.-W. Qiu, W. Ding, Optical pulling forces and their applications. *Adv. Opt. Photonics* **12**, 288 (2020).
34. Q. Song, M. Odeh, J. Zúñiga-Pérez, B. Kanté, P. Genevet, Plasmonic topological metasurface by encircling an exceptional point. *Science* **373**, 1133–1137 (2021).
35. C. W. Hsu, B. Zhen, J. Lee, S. L. Chua, S. G. Johnson, J. D. Joannopoulos, M. Soljačić, Observation of trapped light within the radiation continuum. *Nature* **499**, 188–191 (2013).
36. Q. Song, A. Baroni, P. C. Wu, S. Chenot, V. Brandli, S. Vézian, B. Damilano, P. D. Mierry, S. Khadir, P. Ferrand, P. Genevet, Broadband decoupling of intensity and polarization with vectorial Fourier metasurfaces. *Nat. Commun.* **12**, 3631 (2021).
37. H. Moriceau, F. Rieutord, F. Fournel, Y. le Tiec, L. di Cioccio, C. Morales, A. M. Charvet, C. Deguet, Overview of recent direct wafer bonding advances and applications. *Adv. Nat. Sci. Nanosci. Nanotechnol.* **1**, 043004 (2010).
38. K. Tanaka, D. Arslan, S. Fasold, M. Steinert, J. Sautter, M. Falkner, T. Pertsch, M. Decker, I. Staude, Chiral bilayer all-dielectric metasurfaces. *ACS Nano* **14**, 15926–15935 (2020).
39. T. Stolt, J. Kim, S. Héron, A. Vesala, Y. Yang, J. Mun, M. Kim, M. J. Huttunen, R. Czaplicki, M. Kauranen, J. Rho, P. Genevet, Backward phase-matched second-harmonic generation from stacked metasurfaces. *Phys. Rev. Lett.* **126**, 033901 (2021).
40. M. Z. Alam, I. de Leon, R. W. Boyd, Large optical nonlinearity of indium tin oxide in its epsilon-near-zero region. *Science* **352**, 795–797 (2016).
41. X. Zhang, Y. Liu, J. Han, Y. Kivshar, Q. Song, Chiral emission from resonant metasurfaces. *Science* **377**, 1215–1218 (2022).
42. H. Zhang, X. Sha, Q. Chen, J. Cheng, Z. Ji, Q. Song, S. Yu, S. Xiao, All-dielectric metasurface-enabled multiple vortex emissions. *Adv. Mater.* **34**, 2109255 (2022).
43. M. Kang, L. Mao, S. Zhang, M. Xiao, H. Xu, C. T. Chan, Merging bound states in the continuum by harnessing higher-order topological charges. *Light Sci. Appl.* **11**, 228 (2022).
44. M. Kang, S. Zhang, M. Xiao, H. Xu, Merging bound states in the continuum at off-high symmetry points. *Phys. Rev. Lett.* **126**, 117402 (2021).

Acknowledgments: We would like to thank C. T. Chan for insightful and fruitful discussions. **Funding:** Q.S. acknowledges the funding support from the National Natural Science Foundation of China (no. 12204264), the Shenzhen Stability Support Program (no. WDZC20220810152404001), and the start-up funding in Tsinghua Shenzhen International Graduate School (SIGS), Tsinghua University (no. 01030100006). Y.S. acknowledges the funding support from the National Natural Science Foundation of China (no. 62205246) and the Fundamental Research Funds for the Central Universities. **Author contributions:** H.Q. and Q.S. conceived the idea; H.Q. performed the numerical simulation and calculation; H.Q., Y.S., P.G., and Q.S. wrote the manuscript; Y.S., P.G., and Q.S. supervised and coordinated the project; and all authors discussed the results and approved the paper. **Competing interests:** The authors declare that they have no competing interests. **Data and materials availability:** All data needed to evaluate the conclusions in the paper are present in the paper and/or the Supplementary Materials.

Submitted 7 September 2022
Accepted 28 October 2022
Published 9 December 2022
10.1126/sciadv.ade7556